

Partonic Picture of Nuclear Shadowing at Small x

Zheng Huang, Hung Jung Lu and Ina Sarcevic

Department of Physics, University of Arizona, Tucson, AZ 85721

(May 6, 1997)

We investigate the nuclear shadowing mechanism in the context of perturbative QCD and the Glauber multiple scattering model. Using recent HERA data on nucleon structure function at small x , we put stringent constraints on the nucleon gluon density in the double-logarithm approximation. We suggest that the scaling violation of the nucleon structure function in the region of small x and semihard scale Q^2 can be reliably described by perturbative QCD which is a central key to the understanding of the scale dependence of the nuclear shadowing effect. Our results indicate that while the shadowing of the quark density arises from an interplay between the “soft” and semihard QCD processes, the gluon shadowing is largely driven by a perturbative shadowing mechanism. We demonstrate that the gluon shadowing is a robust phenomenon at large Q^2 and can be unambiguously predicted by perturbative QCD.

PACS numbers: 24.85.+p, 25.75.-q, 12.38.Bx, 13.60.Hb

I. INTRODUCTION

The theoretical studies of semihard processes play an increasingly important role in ultrarelativistic heavy-ion collisions at $\sqrt{s} \geq 200$ GeV in describing the global collision features such as the particle multiplicities and transverse energy distributions. These semihard processes can be reliably calculated in the framework of perturbative QCD and they are crucial for determining the initial condition for the possible formation of a quark-gluon plasma. Assuming the validity of the factorization theorem in perturbation theory, it is essential to know the parton distributions in nuclei in order to compute these processes. For example, to calculate the minijet production for $p_T \sim 2$ GeV or the charm quark production in the central rapidity region ($y = 0$), one needs to know the nuclear gluon structure function, $xg_A(x, Q^2)$, at $Q \sim p_T$ or m_c and $x = x_{Bj} = 2p_T/\sqrt{s}$ or $2m_c/\sqrt{s}$. For $\sqrt{s} \geq 200$ GeV, the corresponding value of x is $x \leq 10^{-2}$. Similarly, the knowledge of nuclear quark density $xf_A(x, Q^2)$ is needed for the Drell-Yan lepton-pair production process.

The attenuation of quark density has been firmly established experimentally in deeply-inelastic lepton scatterings (DIS) from nuclei at CERN [1] and Fermilab [2] in the region of small values of the Bjorken variable $x = Q^2/2m\nu$, where Q^2 is the four-momentum transfer squared, ν is the energy loss of the lepton in the lab frame and m is the nucleon mass. The data, taken over a wide kinematic range $10^{-5} < x < 0.1$ and $0.05 \text{ GeV}^2 < Q^2 < 100 \text{ GeV}^2$, show a systematic reduction of nuclear structure function $F_2^A(x, Q^2)/A$ with respect to the free nucleon structure function $F_2^N(x, Q^2)$. There are also some indications of nuclear gluon shadowing from the analysis of J/Ψ suppression in hadron-nucleus experiments [3]. Unfortunately, the extraction of nuclear gluon density is not unambiguous since it involves the evaluation of initial parton energy loss and final state interactions [4]. These measurements present a tremendous challenge to the theoretical models of nuclear shadowing

(for recent reviews, see [5]).

The partonic description of nuclear shadowing phenomenon has been extensively investigated in literatures in the context of a recombination model [6–8] and a Glauber multiple scattering theory [9–13]. These approaches predict a modified QCD evolution equation for the nuclear structure function in contrast to a Gribov-Lipatov-Altarelli-Parisi (GLAP) evolution equation [14] for nucleon. Qualitatively, the scale (Q^2) evolution of the nuclear structure function in the modified equation is slower than the nucleon case, leading to a perturbative mechanism for the depletion of the parton density at large momentum transfer. The quantitative prediction of nuclear shadowing at large Q^2 in general depends on the initial value of shadowing at small momentum transfer where perturbative calculation breaks down and some non-perturbative model or experimental input is needed. The so-called vector-meson-dominance (VMD) model [15] has been quite successful in predicting the quark shadowing at low Q^2 where the experimental data are rich [1,2]. Presently, there is no viable non-perturbative model for the gluon case and there is very little experimental information on the initial gluon shadowing value at some low Q_0^2 . This, in practice, would make the prediction on gluon shadowing very uncertain.

In this paper, however, we suggest that there exists a typical scale $Q_{SH}^2 \simeq 3 \text{ GeV}^2$ in the perturbative evolution of the nuclear gluon density beyond which the nuclear gluon shadowing can be unambiguously predicted in the context of perturbative QCD. The so-called “semihard” scale Q_{SH}^2 is determined by the strength of the scaling violation of the nucleon gluon density in the small- x region at which the anomalous dimension, $\gamma \equiv \partial \ln xg_N / \ln Q^2$, is of $O(1)$. We shall demonstrate that as Q^2 approaches Q_{SH}^2 , the gluon shadowing ratio rapidly approaches a unique perturbative value determined by the Glauber multiple scattering theory. For $Q^2 > Q_{SH}^2$, the nuclear gluon density, in contrast to the quark case, is almost independent of the initial distribution at Q_0^2 and its evo-

lution is mainly governed by a GLAP equation. The suggested phenomenon is a consequence of the singular growth of the gluon density in the small- x region and the perturbative shadowing caused by the coherent parton multiple scattering.

In particular, we shall present a quantitative study of the scale dependence of the nuclear shadowing phenomenon for both the quark and the gluon distributions based on the Glauber diffractive approximation. A similar study has been performed by Eskola in the recombination model [16]. Our focus is the sensitivity of the nuclear shadowing at large Q^2 to the initial conditions. To determine the gluon content of the nucleon, we shall use a leading double logarithm approximation (DLA) where the scaling violation of the quark structure function F_2^N is entirely caused by a $g \rightarrow q\bar{q}$ splitting. The agreement between our results based on the DLA and the measured values of F_2^N indicates that the perturbative evolution sets in as early as $Q^2 \geq 0.8 \text{ GeV}^2$ and the scaling violation of gluon structure function in the semihard region can be reliably described by the DLA. This provides a basis for studying both the nuclear quark and gluon densities in the Glauber approach where the separation of $q\bar{q}$ or gg pair in the DLA is considered frozen during its passage in the nucleus. The reason for not using the available parton distributions for a nucleon such as those of MRS, CTEQ or GRV parameterization [17] is that the nuclear structure function obtained in our Glauber approach does not contain a full GLAP kernel, as it will become clear below. Since the shadowing ratio depends on both the nuclear and the nucleon structure functions, they should be consistently calculated in the same approximation. We expect that the calculated ratio, however, has a validity beyond the DLA.

We shall demonstrate that the nuclear shadowing for the quark distribution is a leading twist effect due to the interplay between the “soft” and the “semihard” QCD processes, while for the gluon distribution, the shadowing is largely driven by the perturbative shadowing mechanism at small x . Beyond the semihard scale, both quark and gluon shadowing ratios are shown to evolve slowly. We discuss the x -dependence of the shadowing ratio and the non-saturating feature of the perturbative shadowing. As a by-product of the Glauber approach, we also study the nuclear geometry dependence of the shadowing ratio, which cannot be addressed in the recombination model such as the GLR equation. Since the shadowing effect is intimately related to the effective number of scatterings, it should vary strongly as one changes the impact parameter. This leads to the breakdown of the factorization of the nuclear parton density into the product of an impact parameter averaged parton distribution and the nuclear thickness function.

The paper is organized as follows. In section II we discuss the physical picture of the nuclear shadowing phenomenon. It can be regarded as a heuristic introduction

to the central idea of our approach. In section III, we calculate the nucleon structure function $F_2^N(x, Q^2)$ for large range of x and Q^2 using a gluon density obtained in the DLA. We determine the initial condition for F_2^N and for xg_N by fitting the Q^2 -dependence of F_2^N at small value of x . The gluon density in a nucleon is crucial to the nuclear shadowing effect. In section IV we give a brief introduction on the Glauber multiple scattering model and discuss the dependence of the nucleon density on the coherence length of the virtual photon. The nuclear shadowing effect for F_2^A is calculated in section V and the initial shadowing is parameterized in order to fit the available experimental data at the measured Q^2 values. In section VI, the gluon shadowing is computed using the Glauber formula derived by Mueller [12] and Ayala F, Gay Ducati and Levin [13]. Section VII is devoted to the discussion of the impact parameter dependence of the nuclear shadowing. We conclude our findings in section VIII.

II. PHYSICAL PICTURE OF NUCLEAR SHADOWING

At low Q^2 ($< 1 \text{ GeV}^2$) in the deeply-inelastic scattering, the interaction of the virtual photon with the nucleons in the rest frame of the target is most naturally described by a vector-meson-dominance (VMD) model [15], in which the virtual photon interacts with the nucleons via its hadronic fluctuations, namely the ρ , ω and ϕ mesons. The shadowing of the (sea) quark density is caused by the coherent multiple scatterings of the vector meson off the nucleons with a large hadronic cross section σ_{VN} , which can be most conveniently studied in the Glauber diffractive approximation model [18]. The x -dependence of the shadowing ratio, $R(x, Q^2) = F_2^A(x, Q^2)/AF_2^N(x, Q^2)$, is explained by the coherent length of the virtual photon $l_c \simeq 1/2mx$. For $x < 10^{-2}$, $l_c > R_A = 4 \sim 5 \text{ fm}$ for large nuclei, the vector meson interacts coherently with all nucleons inside the nucleus resulting in a uniform (in x) reduction of the total cross section, while for $x > 10^{-2}$, $l_c < R_A$ the vector meson can only interact coherently with a fraction of all the nucleons and shadowing is reduced. The VMD model in general predicts much less scaling violation of $F_2^N(x, Q^2)$ than it has been observed in the small x region and a rapid disappearance of the nuclear shadowing for $Q^2 \gg m_V^2$. Although a generalized VMD model which includes higher resonances may improve the situation somewhat, it is generally believed that the nuclear shadowing in the VMD model is a higher twist effect, which is in contraction with the experimental evidence that the $R(x, Q^2)$ has a rather weak Q^2 dependence [1,2].

At high Q^2 ($> 1 \sim 2 \text{ GeV}^2$), the virtual photon can penetrate the nucleon and probe the partonic degrees of freedom where a partonic interpretation based on pertur-

bative QCD is most relevant in the infinite momentum frame. It is well known that the Q^2 -dependence, the so-called scaling violation of the nucleon structure function $F_2^N(x, Q^2)$ can be well accounted for by the Gribov-Lipatov-Altarelli-Parisi (GLAP) evolution equation [14] given some non-perturbative initial condition $F_2^N(x, Q_0^2)$ [17]. In the small x region, the GLAP equation predicts a strong scaling violation of $F_2^N(x, Q^2)$ due to the strong growth of the gluon density in the nucleon. In fact, a dominant perturbative evolution implies that the growth of $F_2^N(x, Q^2)$ in $\ln Q^2$ at fixed, small x is closely related to the growth in $\ln 1/x$ at fixed Q^2 , i.e. the so-called double scaling violation observed in the DIS experiments for nucleon, most transparent in the Leading-Double-Logarithm Approximation (DLA) of the gluon structure function. At extremely small x , the resummation of large $\ln 1/x$ is necessary leading to the BFKL evolution equation [19] which may also be derived in a Weizsacker-Williams classical field approximation [20]. It is not clear when the BFKL hard pomeron will become relevant since the GLAP evolution seems able to describe most of kinematical region that current experiments have probed so far. As we shall show, the main feature of the Q^2 -dependence of the nuclear shadowing is intimately related to this strong scaling violation in the small- x region.

If the nuclear structure function follows the same perturbative GLAP evolution, given an initially shadowed $F_2^A(x, Q_0^2)$, the shadowing ratio $R(x, Q^2)$ as Q^2 increases will quickly approach 1 because of the strong scaling violation $F_2^A(x, Q^2) \gg F_2^A(x, Q_0^2)$. This would imply that the shadowing is purely non-perturbative and thus a higher twist effect. The key observation is that in the infinite momentum frame, because of the high nucleon and parton densities, the quarks and gluons that belong to different nucleons in the nucleus will recombine and annihilate, leading to the so-called recombination effect first suggested by Gribov, Levin and Ryskin [6] and later proven by Mueller and Qiu [7]. In the target rest frame, the virtual photon interacts with nucleons via its quark-antiquark pair ($q\bar{q}$) color-singlet fluctuation [10]. If the coherence length of the virtual photon is larger than the radius of the nucleus, $l_c > R_A$, the $q\bar{q}$ configuration interacts coherently with all nucleon with a cross section given by the color transparency mechanism for a point like color-singlet configuration [21]. That is, the cross section is proportional to the transverse separation squared, r_t^2 , of the q and \bar{q} . In the double logarithm approximation (DLA), the cross section can be expressed through the gluon structure function for a nucleon

$$\sigma_{q\bar{q}N} \propto r_t^2 \alpha_s x' g_{\text{DLA}}(x', 1/r_t^2), \quad (2.1)$$

where $x' = M^2/2m\nu$ and M is the invariant mass of $q\bar{q}$ pair. The total cross section $\sigma_{q\bar{q}A}$ can be calculated in the Glauber eikonal approximation,

$$\sigma_{q\bar{q}A} = \int d^2b 2\{1 - e^{-\sigma_{q\bar{q}N} T_A(b)/2}\}, \quad (2.2)$$

where b is the impact parameter and $T_A(b)$ is the nuclear thickness function. The nuclear cross section is therefore reduced when compared to the simple addition of free nucleon cross sections.

However, it is not clear that (2.1) and (2.2) will provide a satisfactory explanation of the non-vanishing shadowing effect at large Q^2 . Although for a given Q^2 , all $q\bar{q}$ configurations with the separation size $r_t^2 > 1/Q^2$ are possible, the virtual photon wavefunction $|\psi_{\gamma^*}|^2 \sim 1/r_t^2$ favors the smallest value of $r_t^2 \simeq 1/Q^2$ where the cross section is small and no significant shadowing would be expected. The resolution to this problem comes from the fact that the nucleon structure function exhibits a strong scaling violation in the small x region at the moderate (semihard) momentum transfer $0.8 \text{ GeV}^2 < Q^2 < Q_{\text{SH}}^2$ where $Q_{\text{SH}}^2 \simeq 3 \text{ GeV}^2$. As we shall show, the strong scaling violation in this region can be understood in the context of perturbative QCD. The gluon density in (2.1) grows rapidly with $1/r_t^2$ in the small x region, which can compensate the inherent “smallness” of the cross sections of “hard” QCD processes. As a consequence, the semihard processes can compete successfully with the “soft” processes as described in the VMD model and continue to provide the shadowing mechanism up to some moderately high value of $Q^2 \sim Q_{\text{SH}}^2$. In terms of the anomalous dimension $\gamma(Q^2) = d \ln x g_N / d \ln Q^2$, the cross section in (2.1) may be effectively expressed as

$$\sigma_{q\bar{q}N} \propto \frac{(Q^2)^\gamma}{Q^2}. \quad (2.3)$$

The large anomalous dimension, $\gamma > 1$, even at moderately large Q^2 delays the rapid falling of the cross section due to the “smallness” of the configuration size, as first argued by Gribov, Levin and Ryskin in [6]. We refer to this as the perturbative shadowing mechanism as it can be computed in perturbative QCD. At even higher values of Q^2 , $Q^2 > Q_{\text{SH}}^2$, the scaling violation becomes weak (logarithmic), and the perturbative shadowing mechanism ceases to be effective. In this case, both the nucleon and the nuclear structure function evolve slowly at the same rate. The shadowing ratio developed by both perturbative and non-perturbative mechanisms in the relatively low- Q^2 region persists in the high- Q^2 region but tends to 1 rather slowly as $Q^2 \rightarrow \infty$.

In contrast to the VMD model, the x -dependent cross section $\sigma_{q\bar{q}N}$ predicts an additional x -dependence of the shadowing ratio apart from the coherence length dependence in the perturbative region. As a result, one does not in general expect the saturation of the shadowing ratio as x decreases below the coherence limit $x < 10^{-2}$. On the other hand, as Q^2 decreases, the gluon distribution changes from a singular small- x behavior (hard pomeron regime) to the less singular one (soft pomeron)

regime). The shadowing ratio becomes flatter as Q^2 decreases. The observed saturation of the shadowing ratio in the small- x region [2] is thus a non-perturbative, low- Q^2 feature.

Similarly, the nuclear gluon density may be studied by considering a deeply-inelastic scattering of a virtual colorless probe (e.g. the virtual ‘‘Higgs boson’’) with the nucleus where the interaction proceeds via a gluon pair (gg) component of the virtual probe. This has been introduced by Mueller [12] and recently studied by Ayala F, Gay Ducati and Levin (AGL) [13]. In contrast to the quark distribution, the gluon structure functions for nucleon and nucleus are poorly known, especially in the small- x region. They are both of extreme importance for the semihard QCD processes at high energies. Most of our knowledge about the gluon distribution comes from the theoretical expectations based on perturbative QCD constrained by the scaling violation of F_2^N and the prompt photon experiments [17]. The nuclear gluon density may also be studied in the Glauber multiple scattering model where $\sigma_{q\bar{q}N}$ in (2.2) is to be replaced by σ_{ggN} . Simple color group representation argument relates these two cross sections by $\sigma_{ggN} = 9\sigma_{q\bar{q}N}/4$. However, what makes the gluon case very different from the quark case is the unknown initial (non-perturbative) gluon density in the nucleus. There is very little experimental information on the gluon shadowing at low Q^2 and small x . The VMD model is not applicable here since the low-lying meson spectroscopy for gg -like states is poorly known. This would make this approach very uncertain in predicting the amount of gluon shadowing in the nucleus.

However, as we shall show in this paper, the larger cross section σ_{ggN} implies an even stronger scaling violation of gluon density than the quark case, making the perturbative shadowing a dominant mechanism. As a consequence, the shadowing ratio is largely determined by the perturbative calculation at $Q^2 = Q_{\text{SH}}^2$. That is, the large anomalous dimension of gluon distribution function for a nucleon drives the shadowing ratio rapidly to approach the perturbative value at moderately large $Q^2 = Q_{\text{SH}}^2$ and the influence of an initial shadowing at low Q^2 becomes relatively unimportant. For $Q^2 > Q_{\text{SH}}^2$, the scaling violation becomes weaker, the shadowing ratio determined by the perturbative shadowing mechanism at the semihard scale persists and evolves slowly. The x -dependence of the shadowing ratio can be also predicted to be non-saturating, a generic feature of the perturbative shadowing. We therefore suggest that the nuclear gluon shadowing at $Q^2 > Q_{\text{SH}}^2 \simeq 3 \text{ GeV}^2$ and at small x can be predicted in the context of perturbative QCD. The prediction is based on the scaling violation of the gluon structure function and the existence of the perturbative shadowing in the Glauber multiple scattering model.

III. LAB FRAME DESCRIPTION OF NUCLEON STRUCTURE FUNCTION

Since the nuclear shadowing ratio depends sensitively on the nucleon structure function, we shall develop a formalism to calculate both the nuclear and the nucleon structure functions simultaneously in order to reduce the uncertainty due to the nucleon structure function. This prevents us from using the well-known parametrizations such as MRS, CTEQ and GRV [17] which are based on the full next-to-leading-order GLAP equation because the nuclear structure function is not derived in the same formalism. We stress that the shadowing is only a few tens percentage effect, thus the uncertainty in the nucleon structure function at the same level can cause a large effect on the shadowing ratio.

A. Quark Distribution

Consider a description of deeply-inelastic lepton scattering off a nucleon in the laboratory frame. The inclusive cross section can be expressed via the virtual photon-nucleon total cross section. The cross section for the absorption of a virtual photon in the small x region is dominated by the scattering off the sea-quark $q\bar{q}$ pair. The generic perturbative QCD diagrams giving rise to the $q\bar{q}$ fluctuation are shown in Fig. 1. The CM energy of the incoming virtual photon at small x is

$$s = (q + p)^2 \simeq 2p \cdot q = \frac{Q^2}{x}, \quad (3.1)$$

where q and p are the four-momenta of the photon and the target nucleon. Thus a region of small x corresponds to a high energy scattering process at fixed Q^2 .

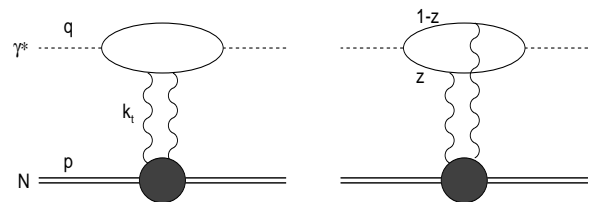


FIG. 1. The perturbative diagrams giving rise to the $q\bar{q}$ pair fluctuation.

The imaginary part of the amplitudes in Fig. 1 is related to the photoabsorption cross section which has been calculated by Nikolaev and Zakharov [11] assuming that the size of the $q\bar{q}$ pair is frozen in the scattering process and that the one-gluon exchange process dominates. This is nothing but the so-called double logarithm approximation (DLA) [6,22]. The transverse cross section can be cast into an impact parameter representation

$$\sigma(\gamma^* N) = \int_0^1 dz \int d^2\mathbf{r} |\psi(z, \mathbf{r})|^2 \sigma_{q\bar{q}N}(\mathbf{r}), \quad (3.2)$$

where z is the Sudakov variable, defined to be the fraction of the $q\bar{q}$ pair momentum carried by one of the (anti)quarks, \mathbf{r} is the variable conjugate to the transverse momentum of (anti)quark of the pair, representing the transverse size of the pair. $\psi(z, \mathbf{r})$ can be interpreted as the wave function of the $q\bar{q}$ fluctuations of virtual photon. Thus, $|\psi(z, \mathbf{r})|^2$ serves as the probability of finding a $q\bar{q}$ pair with a separation \mathbf{r} and a fractional momentum z . In an explicit form

$$|\psi(z, \mathbf{r})|^2 = \frac{6\alpha_{\text{em}}}{(2\pi)^2} \sum_1^{N_f} e_i^2 P(z) a^2 K_1(ar)^2, \quad (3.3)$$

where $a^2 = Q^2 z(1-z)$ and K_1 is the modified Bessel function. The factor $P(z) = z^2 + (1-z)^2$ is the universal splitting function of gauge boson into the fermion pair. Since K_1 is a rapidly falling function, the integral in (3.2) has important contributions only in the region $ar \ll 1$. In this case, one has

$$|\psi(z, \mathbf{r})|^2 \rightarrow \frac{6\alpha_{\text{em}}}{(2\pi)^2} \sum_1^{N_f} e_i^2 \frac{1}{r^2}, \quad (3.4)$$

where the expansion $K_1(ar)^2 \rightarrow 1/a^2 r^2$ has been used. The photon wave function favors a $q\bar{q}$ pair with small transverse separation.

The cross section for the high energy interaction of a small-size $q\bar{q}$ configuration with the nucleon can be unambiguously calculated in QCD in the region of small x by applying the QCD factorization theorem. In the DLA, the result is [23]

$$\sigma_{q\bar{q}N}(\mathbf{r}) = \frac{\pi^2}{3} r^2 \alpha_s(Q'^2) x' g_N^{\text{DLA}}(x', Q'^2), \quad (3.5)$$

where $x g_N^{\text{DLA}}$ is the gluon distribution of the nucleon calculated in the DLA. The fact that the cross section is proportional to the size of the point-like configuration is the consequence of the color transparency in QCD. Although the r^2 factor in (3.5) decreases fast as one goes to the short distance, the singular behavior of the wave function in (3.4) and the strong scaling violation of $x g_N^{\text{DLA}}$ in the small- x region as r decreases can compensate the smallness of cross section due to the color transparency. As a result, the soft and hard physics compete in a wide range of Q^2 .

The x' and Q'^2 in (3.5) are related to z , x and r^2 as follows. The invariant mass squared of the $q\bar{q}$ pair is

$$M^2 \simeq \frac{k_t^2}{z(1-z)}, \quad (3.6)$$

where $k_t^2 \simeq 1/r^2$ is the transverse momentum squared of the (anti)quark. The virtuality of the gluon is then $Q'^2 = (k_t - (-k_t))^2 = 4/r^2$ while x' is given by

$$x' = \frac{M^2}{2m\nu} = \frac{k_t^2}{z(1-z)2m\nu} \simeq \frac{x}{a^2 r^2}, \quad (3.7)$$

where ν is the energy loss of the lepton. The condition $ar < 1$ implies $x' > x$. Since $r^2 > 4/Q^2$, the integration region in z is limited by $a^2 r^2 = Q^2 r^2 z(1-z) < 1$. Because the integrand in (3.2) is symmetric under $z \leftrightarrow 1-z$, one has $\int_0^1 dz \rightarrow 2 \int_0^\epsilon dz$ where ϵ is the solution to $ar = 1$ or $x' = x$.

At small x , the free nucleon structure function can be written in terms of the virtual photon-nucleon cross section

$$F_2^N(x, Q^2) = \sum_i e_i^2 x f_N(x, Q^2) = \frac{Q^2 \sigma(\gamma^* N)}{4\pi^2 \alpha_{\text{em}}}, \quad (3.8)$$

where $x f_N(x, Q^2)$ is the (sea) quark distribution function. Substituting (3.2) into the above equation and changing the integration variable z into x' in (3.2) $dz = -x dx' / (x'^2 Q^2 r^2)$, one obtains

$$f_N(x, Q^2) = f_N(x, Q_0^2) + \frac{3}{4\pi^3} \int_x^1 \frac{dx'}{x'^2} \times \int_{4/Q^2}^{4/Q_0^2} \frac{dr^2}{r^4} \sigma_{q\bar{q}N}(x', r^2), \quad (3.9)$$

where $\sigma_{q\bar{q}N}$ is given in (3.5). We have split the integration on r^2 into the region $4/Q^2 < r^2 < 4/Q_0^2$ where the perturbative calculation is valid and the region $r^2 > 4/Q_0^2$ where the perturbation theory breaks down and the cross section is not calculable. The non-perturbative part is taken as an initial condition $f_N(x, Q_0^2)$ which should be determined by the experimental measurement. However, it is worthwhile to emphasize that because of the exponential cutoff of the large r^2 by $K_1(ar)^2$ in (3.2), the integration in r^2 is infrared safe. Even if one substitutes the small- r cross section into (3.9), the integral is only logarithmically divergent $\sim \ln Q_0^2$, in contrast to the usual factorization scheme of the hard process. This allows a smooth extrapolation of the ‘‘semihard’’ physics into the ‘‘soft’’ physics. Thus one can choose a rather small cutoff Q_0^2 in order to integrate more perturbative contributions. Because of the infrared safety, the uncertainty due to the choice of Q_0^2 is minimal.

Substituting (3.5) into (3.9) and replacing $4/r^2$ by Q'^2 , one recovers the familiar integrated form of the GLAP evolution equation at small x

$$f_N(x, Q^2) = f_N(x, Q_0^2) + \frac{1}{4\pi} \int_x^1 \frac{dx'}{x'} \times \int_{Q_0^2}^{Q^2} \frac{dQ'^2}{Q'^2} \alpha_s(Q'^2) g_N^{\text{DLA}}(x', Q'^2). \quad (3.10)$$

Note that (3.10) is not an integral equation since it does not involve the sea-quark contribution on the right hand side. It is derived in the DLA where the small- x behavior is driven by the gluon contribution. To improve the larger x behavior, we insert a splitting function $P_{gq}(z) = z^2 +$

$(1-z)^2$ where $z = x/x'$ in (3.10) and add the valence quark contributions to F_2^N

$$F_2^N(x, Q^2) = \sum_i e_i^2 [x f_N(x, Q^2) + x v_i(x, Q^2)], \quad (3.11)$$

where xv 's are the valence quark distributions, which are given by the GRV [17] parameterization (there is a very little difference among different parameterizations for valence quarks).

B. Scaling Violation of $F_2^N(x, Q^2)$ and Gluon Density

The Q^2 evolution or the scaling violation of the nucleon gluon density in the small- x region is quite different from that in the large- x region in the context of GLAP equation. In the region of small x , one has to sum up large $\alpha_s \ln 1/x$ contributions in addition to $\alpha_s \ln Q^2$ terms represented by the ladder diagrams with strong scale ordering in the leading logarithm approximation (LLA). To avoid summing up two large logarithms, one considers the DLA, i.e., the most leading diagrams involving $(\alpha_s \ln Q^2 \ln 1/x)^n$ at each order n . Such a double logarithm appears only when vector particles (gluons) propagate in the t -channel of the ladder diagram as argued by Gribov, Levin and Ryskin in [6]. Thus, the scale dependence of the nucleon quark distribution is directly related to the small- x behavior of the gluon distribution.

In general, the DLA is valid in the kinematical region where $\alpha_s \ln 1/x \ln Q^2/Q_0^2 \sim 1$ while $\alpha_s \ln 1/x \ll 1$ and $\alpha_s \ln Q^2/Q_0^2 \ll 1$ as well as $\alpha_s \ll 1$. The precise validity range of DLA or of GLAP equation is currently still under debate. The general belief is that it describes a region up to a moderately large Q^2 ($\sim 20 \text{ GeV}^2$) and a moderately small x , $10^{-5} < x < 10^{-2}$. Formally, in the small- x region, one should sum the large $\alpha_s \ln 1/x$ terms using a BFKL resummation technique [19]. However, it has been shown recently by Ball and Forte [22] that a gluon density obtained in the DLA together with the resummed leading logarithm in Q^2 gives a very good description of the double-asymptotic scaling observed at HERA [24]. The unitarized gluon density in the DLA has a simple approximate form [6,22],

$$xg_N^{\text{DLA}} = xg_N(x, Q_0^2)I_0(y), \quad (3.12)$$

where I_0 is the Bessel function and

$$y = 2c \sqrt{\ln\left(\frac{1}{x}\right) \ln\left(\frac{t}{t_0}\right)}, \quad (3.13)$$

with $t \equiv \ln Q^2/\Lambda^2$ and $c = \sqrt{36/25}$, provided that input $xg_N(x, Q_0^2)$ is not singular in x . The asymptotic behavior of $I_0(y)$ is that $I_0(y) \rightarrow 1$ as $y \rightarrow 0$ and $I_0(y) \rightarrow e^y/\sqrt{2\pi y}$ as $y \rightarrow \infty$. That is, in this DLA, xg_N increases faster than any power of $\ln 1/x$, but slower than a power of

$1/x$. To improve the DLA at a large Q^2 ($> 20 \text{ GeV}^2$), the resummation of single logarithm, $\alpha_s \ln Q^2/Q_0^2$, is necessary. This results in an additional Q^2 dependence of the gluon distribution, a multiplicative factor $(t/t_0)^{-\delta}$ in (3.12) where $\delta = 61/45$ [22]. We find that this modification has very little numerical effect on the nuclear shadowing ratio in the region of interest.

In a semiclassical form $xg_N = x^{-\omega}(Q^2)^\gamma$. One defines the exponents $\gamma = \partial \ln xg_N/\partial t$ and $\omega = \partial xg_N/\partial \ln(1/x)$. In the DLA,

$$\gamma = \frac{\ln 1/x}{t \ln t/t_0} \omega. \quad (3.14)$$

The anomalous dimension can be large in the small- x and $-t$ region. As $t \rightarrow t_0$, $\omega \rightarrow 0$ and γ is finite. It is important to emphasize that the DLA form (3.12) is only valid when $Q^2 \gg Q_0^2$.

Our goal is to pin down the gluon density in the nucleon. In our approach, the slope of F_2^N in Q^2 , $dF_2^N/d \ln Q^2$, is virtually a direct indicator of the magnitude of the gluon distribution. We require that the gluon distribution in the DLA as given in (3.12) describes reasonably well the scaling violation of F_2^N for Q^2 ranging from 0.85 GeV^2 to 100 GeV^2 where the experimental data exist in the small- x region. As it is turned out, this almost uniquely determines the gluon distribution.

There are two unknown quantities in (3.12): Q_0^2 and the initial condition $xg_N(x, Q_0^2)$. Q_0^2 determines where the perturbative calculation should begin to be valid and where the non-perturbative contribution can be separated into an initial condition $xg_N(x, Q_0^2)$. We would like to have a reliable perturbative description of the structure function in the range from 1 to a few GeV which is extremely important in understanding the evolution of nuclear shadowing. This leads to choosing Q_0^2 to be rather small so that the DLA sets in at a relatively low $Q^2 = 1 \sim 2 \text{ GeV}^2$. Since $xg_N(x, Q_0^2)$ has to be non-singular in the small x regime, we take $xg_N(x, Q_0^2) = c_g xg_N^{\text{GRV}}(x, Q_0^2)$ at an initial scale Q_0^2 since the initial gluon distribution in GRV is fairly flat while it has the proper behavior at $x \rightarrow 1$. The initial condition for F_2^N is taken to be in the form motivated by a soft pomeron with an intercept $\alpha = 1 + 0.08$ [25]

$$F_2^N(x, Q_0^2) = c_P x^{-0.08} (1-x)^\eta, \quad (3.15)$$

where $\eta = 10$ accounts for the behavior as $x \rightarrow 1$. We determine Q_0^2 , c_g and c_P by requiring that the calculated Q^2 -dependence of F_2^N at $x = 8 \times 10^{-5}$ fits the recent measurement from H1 Collaboration [24]. We find the following unique solution

$$Q_0^2 = 0.4; \quad c_g = 2.2; \quad c_P = 0.2. \quad (3.16)$$

The Q^2 -dependence of F_2^N at other values of small x are then predicted using (3.10). In Fig. 2, we show our results

for F_2^N compared to the experimental values [24]. The gluon density in (3.12) describes the scale dependence of F_2^N very well starting at a relatively low Q^2 , $Q^2 \sim 0.85$ GeV².

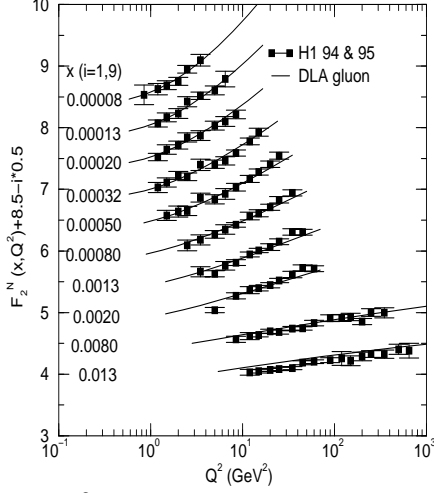


FIG. 2. The Q^2 -dependence of the nucleon structure function calculated using the DLA and compared with experiment data [24].

The x -dependence of the nucleon structure function can also be predicted from (3.10). Fig. 3 shows the calculated $F_2^N(x, Q^2)$ from (3.10) as function of x at various Q^2 as compared to H1 measured values [24]. The agreement is evident. Starting with a fairly flat distribution $F_2^N(x, Q_0^2)$, the nucleon structure function develops a more and more singular shape in x from the perturbative evolution governed by the gluon distribution. Some deviation is visible for $x > 10^{-2}$, a region where we do not expect DLA to be valid.

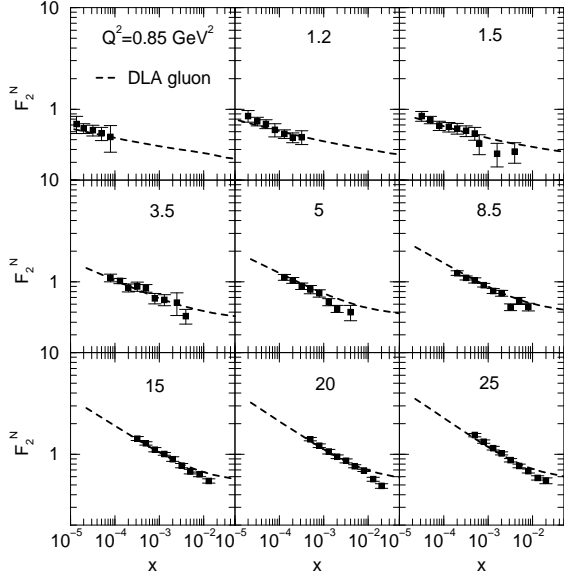


FIG. 3. The x -dependence of the nucleon structure function calculated using the DLA and compared with the experiment data.

The results shown in Fig. 2 and Fig. 3 demonstrate that the gluon density in the DLA given in (3.12) faithfully captures the essential feature of Q^2 - and x -evolution of the nucleon structure function. The fact that we can describe F_2^N even at very low Q^2 , $0.85 < Q^2 < 5$ GeV² indicates that the perturbative approach is reliable in the semihard region.

C. Gluon Distribution in the DLA

Similarly to the quark case, one can consider the virtual gg pair interacting with the nucleons in the nuclear target. Using the well-known relationship between the gluon density and the deeply-inelastic cross section [12], the gluon density can be written as [13]

$$xg_N(x, Q^2) = \frac{2}{\pi^4} \int_0^1 dz \int d^2\mathbf{r} |\psi(z, \mathbf{r})|^2 \sigma_{ggN}(\mathbf{r}), \quad (3.17)$$

where the wave function squared for a gluon pair is

$$|\psi(z, \mathbf{r})|^2 = \frac{1}{z(1-z)} \left[(a^2 K_2(ar) - aK_1(ar)/r)^2 + a^2 K_1(ar)^2 / r^2 \right] \overset{ar \ll 1}{\sim} \frac{2}{zr^4}, \quad (3.18)$$

and the cross section in the DLA is [23]

$$\sigma_{ggN}(\mathbf{r}) = \frac{3\pi^2}{4} r^2 \alpha_s(4/r^2) x' g_N^{\text{DLA}}(x', 4/r^2). \quad (3.19)$$

Note $\sigma_{ggN} = 9\sigma_{q\bar{q}N}/4$. Substituting (3.18) and (3.19) into (3.17), one obtains

$$g_N(x, Q^2) = g_N(x, Q_0^2) + \frac{1}{2\pi} \int_x^1 \frac{dx'}{x'} \int_{Q_0^2}^{Q^2} \frac{dQ'^2}{Q'^2} \times \alpha_s(Q'^2) \left(6 \frac{x'}{x} \right) g_N^{\text{DLA}}(x', Q'^2), \quad (3.20)$$

a form in which the small- x limit splitting function in the DLA can be easily identified: $P_{gg}(z) \simeq 6/z$ where $z = x/x'$. Comparing (3.20) with (3.10), one finds that due to different splitting functions, the gluon density increases as Q^2 increases 12 times faster than the quark density, leading to a much stronger scaling violation. Similar to the quark case, (3.20) is not to be interpreted as the integral equation since the right hand side does not contain g_N but g_N^{DLA} . Namely, g_N^{DLA} is the gluon density seen by a gg pair with a frozen transverse separation while g_N is the gluon density seen by the probe, e.g., the virtual Higgs boson. However, since the integration kernel in (3.20) coincides with that of the DLA evolution equation, g_N should be very close to g_N^{DLA} . We confirm that numerically they differ only by few percent.

IV. GLAUBER MULTIPLE-SCATTERING MODEL

The Glauber multiple-scattering theory [18] treats a nuclear collision as a succession of collisions of the probe with individual nucleons within nucleus. A partonic system (h), being a $q\bar{q}$ or a gg fluctuation, can scatter coherently from several or all nucleons during its passage through the target nucleus. The interference between the multiple scattering amplitudes causes a reduction of the hA cross section compared to the naive scaling result of A times the respective hN cross section, the origin of the nuclear shadowing. In the high-energy eikonal limit, the phase shift of the elastic hA scattering amplitude is just the sum of phase shifts of individual hN scatterings. The total hA cross section is determined by the imaginary part of the forward elastic scattering amplitude as governed by the unitarity relation or the optical theorem. The unitarity of the total cross section is thus built-in within the Glauber theory.

In the high-energy eikonal limit where the projectile's momentum \mathbf{k} is much larger than the inverse of the interaction radius, one describes the scattering amplitude by the Fourier transformation of the so-called profile function $\Gamma(\mathbf{b})$ in the impact parameter space

$$f(\mathbf{k}, \mathbf{k}') = \frac{ik}{2\pi} \int d^2\mathbf{b} e^{i(\mathbf{k}-\mathbf{k}')\cdot\mathbf{b}} \Gamma(\mathbf{b}), \quad (4.1)$$

where \mathbf{k}' is the outgoing wave momentum. In the high energy scattering process, the collision is almost completely absorptive corresponding to an approximately real $\Gamma(\mathbf{b})$ and pure imaginary amplitude. The total cross section is given by the optical theorem

$$\sigma_{\text{tot}} = \frac{4\pi}{k} \text{Im} f(0) = 2 \int d^2\mathbf{b} \Gamma(\mathbf{b}). \quad (4.2)$$

To extend these results to nuclei, one assumes that each collision with the nucleon modifies the piece of the incident wave passing through it by a factor $1 - \Gamma_N(\mathbf{b} - \mathbf{s})$ where \mathbf{s} is the transverse position of the nucleon. The overall modification of the wave is thus given by

$$\prod_{i=1}^A [1 - \Gamma_N(\mathbf{b} - \mathbf{s}_i)]. \quad (4.3)$$

Clearly, only those nucleons in the vicinity of impact parameter \mathbf{b} can influence Γ_A . The nucleus profile function is just the factor in (4.3) multiplied by the probability of finding nucleons in the positions $\mathbf{r}_1, \dots, \mathbf{r}_A$

$$|\psi(\mathbf{r}_1, \dots, \mathbf{r}_A)|^2 = \prod_{i=1}^A \rho(\mathbf{r}_i), \quad (4.4)$$

where $\rho(\mathbf{r}_i)d^3\mathbf{r}_i$ is the probability of finding a nucleon at \mathbf{r}_i . The nucleon number density is then $\rho_A(\mathbf{r}) = \sum_i \rho(\mathbf{r}_i)$. For large A , the nucleus profile is calculated

$$\begin{aligned} \Gamma_A(\mathbf{b}) &= 1 - \prod_{i=1}^A \int d^3\mathbf{r}_i \rho(\mathbf{r}_i) [1 - \Gamma_N(\mathbf{b} - \mathbf{s}_i)] \\ &= 1 - \prod_{i=1}^A [1 - \int d^3\mathbf{r}_i \rho(\mathbf{r}_i) \Gamma_N(\mathbf{b} - \mathbf{s}_i)] \\ &= 1 - \left[1 - \frac{1}{A} \int d^2\mathbf{s} dz \rho_A(\mathbf{s}, z) \Gamma_N(\mathbf{b} - \mathbf{s}) \right]^A \\ &\simeq 1 - \exp \left[- \int d^2\mathbf{s} T_A(\mathbf{s}) \Gamma_N(\mathbf{b} - \mathbf{s}) \right], \end{aligned} \quad (4.5)$$

where we have used $A \gg 1$. We shall use a Gaussian parameterization of the nucleus thickness function defined by

$$T_A(\mathbf{b}) \equiv \int dz \rho_A(\mathbf{b}, z) = \frac{A}{\pi R_A^2} e^{-b^2/R_A^2}, \quad (4.6)$$

where the mean nucleus radius $R_A^2 = 0.4R_{WS}^2$ and $R_{WS} = 1.3A^{1/3}$ fm.

Since the nucleon has a smaller transverse size than the typical nuclear dimension, one approximates the nucleon profile function in (4.5) by $\Gamma_N(\mathbf{b} - \mathbf{s}) \simeq \sigma_{hN} \delta^2(\mathbf{b} - \mathbf{s})/2$ and obtains the total hA cross section

$$\sigma_{hA} = \int d^2\mathbf{b} 2 \left[1 - e^{-\sigma_{hN} T_A(\mathbf{b})/2} \right]. \quad (4.7)$$

For a Gaussian parametrization of $T_A(\mathbf{b})$, the integration on the impact parameter can be done exactly leading to

$$\begin{aligned} \sigma_{hA} &= 2\pi R_A^2 \left[\kappa_h - \frac{1}{4}\kappa_h^2 + \dots + (-1)^{n-1} \frac{\kappa_h^n}{nn!} + \dots \right] \\ &= 2\pi R_A^2 [\gamma + \ln \kappa_h + E_1(\kappa_h)], \end{aligned} \quad (4.8)$$

where $\kappa_h = A\sigma_{hN}/(2\pi R_A^2)$, $\gamma = 0.5772$ is Euler's constant and $E_n(x)$ is the exponential integral function of rank n . The dimensionless quantity κ_h serves as an impact parameter averaged effective number of scatterings. For small value of κ_h , $\sigma_{hA} \rightarrow 2\pi R_A^2 \kappa_h = A\sigma_{hN}$, the total hA cross section is proportional to A or the nuclear volume. In the limit $\kappa_h \rightarrow \infty$, the destructive interference between multiple scattering amplitudes reduces the cross section to $\sigma_{hA} \rightarrow 2\pi R_A^2 (\gamma + \ln \kappa_h)$. Namely, the effective number of scatterings is large and the total cross section approaches the geometric limit $2\pi R_A^2$, a surface term which varies roughly as $A^{2/3}$. In the kinematical region that we are interested in none of these limits are actually approached. The shadowing effect is determined by the strength of κ_h , which is different for a $h = q\bar{q}$ than for a $h = gg$ case.

So far we have sketched the necessary assumptions for applying the Glauber theory for the elastic or the quasielastic scattering, that is, the longitudinal momentum remains the same during the passage of h through the nucleus. This condition can be relaxed to the forward production processes where there is a longitudinal

momentum transfer appropriate to the $q\bar{q}$ or the gg pair production. In this case, the scattering amplitude in (4.1) is modified to include the integration of the longitudinal position z due to the fact that an incident wave $e^{ik_z^\gamma z}$ for the photon γ is changed to a final wave $-\Gamma(\mathbf{b})e^{ik_z^h z}$ for particle h . In general, $k_z^\gamma \neq k_z^h$, and there is a phase difference between the γ and h waves behind the target, i.e., $e^{i\Delta k_z z}$ where $\Delta k_z = k_z^\gamma - k_z^h$. This leads to a coherence length cutoff which is governed by $l_c \simeq 1/\Delta k_z$. If $l_c > R_A$, the hadronic fluctuation h interacts coherently with all nucleons within the nucleus and the Glauber theory is valid. On the other hand, if $l_c < R_A$, h interacts coherently only with some of the nucleons and the interference effect is reduced.

To estimate the coherence length l_c , one calculates the change of the longitudinal momenta in the small- x region

$$\begin{aligned} \Delta k_z &= \sqrt{\nu^2 + Q^2} - \sqrt{\nu^2 - M^2} \\ &\simeq \frac{Q^2 + M^2}{2\nu} = (x + x')m, \end{aligned} \quad (4.9)$$

where M is the invariant mass of the $q\bar{q}$ or the gg pair as defined in (3.7). Since the cross section is dominated by x' near x , the coherence length $l_c \simeq 1/(2xm)$ exceeds the radius of heavy nuclei $R_A \sim 4$ fm as long as $x < 2 \times 10^{-2}$ and the Glauber multiple scattering model is adequate. For $x > 2 \times 10^{-2}$, the Glauber approximation breaks down and one should take into account the finite coherence length. Although we are mainly concerned with the small- x behavior of the nuclear shadowing, we would like to get some handle on the coherence length cutoff in the moderately large- x region. We propose to take a probability approach [13,26] and introduce a coherence length form factor $\tau(\Delta k_z) = \exp[-R_A^2(\Delta k_z)^2/4]$ [13] while preserving the nice structure of the Glauber formula. The probability for a double scattering is reduced by τ , and that for a n -scattering is reduced by τ^{n-1} so that one may make the following replacement in (4.7)

$$2 \left[1 - e^{-\sigma_{hN} T_A(\mathbf{b})/2} \right] \rightarrow \frac{2}{\tau} \left[1 - e^{-\sigma_{hN} T_A(\mathbf{b})\tau/2} \right]. \quad (4.10)$$

As $\tau \rightarrow 1$, the original Glauber formula is preserved, while as $\tau \rightarrow 0$, (4.10) gives $\sigma_{hA} = A\sigma_{hN}$, i.e., there is no shadowing. In the kinematical region $x < 10^{-2}$, the coherence length cutoff does not play a role. Even for $x > 10^{-2}$, because the cross section is already very small, the effect is not very large.

V. NUCLEAR QUARK DISTRIBUTION F_2^A

We now examine the effect of the gluon density in (3.12) on the shadowing of the nuclear structure function. Replacing σ_{hN} in (3.9) and (3.17) by σ_{hA} as calculated by the Glauber multiple scattering model, one obtains for (sea)quarks

$$\begin{aligned} x f_A(x, Q^2) &= x f_A(x, Q_0^2) + \frac{3R_A^2}{8\pi^2} x \int_x^1 \frac{dx'}{x'^2} \int_{Q_0^2}^{Q^2} dQ'^2 \\ &\quad \times \frac{1}{\tau} [\gamma + \ln(\kappa_q \tau) + E_1(\kappa_q \tau)], \end{aligned} \quad (5.1)$$

where the effective number of scatterings κ is given by

$$\kappa_q(x, Q^2) = \frac{2A\pi}{3R_A^2 Q^2} \alpha_s(Q^2) x g_N^{\text{DLA}}(x, Q^2), \quad (5.2)$$

Expanding $[\dots]$ in (5.1) and keeping only the first term which is proportional to κ_q , one recovers the results for the nucleon in the same DLA approximation.

The nuclear structure function $F_2^A(x, Q^2)$ is defined through the total γ^* - A cross section, similar to F_2^N in (3.8). To improve the large- x behavior, we add to F_2^A the valence quark contributions and assume that there is no shadowing for the valence quarks

$$F_2^A(x, Q^2) = \sum_i e_i^2 [x f_A(x, Q^2) + A x v_i(x, Q^2)]. \quad (5.3)$$

In principle, the initial condition $x f_A(x, Q_0^2)$ in (5.1) may be calculated in the vector-meson-dominance (VMD) model. Fortunately, there have been some experimental measurements on the nuclear quark shadowing in the low- Q^2 region so that the initial condition can be expressed in terms of the production of the initial nucleon structure function and the shadowing ratio $R_0^q(x)$

$$F_2^A(x, Q_0^2) = A R_0^q(x) F_2^N(x, Q_0^2), \quad (5.4)$$

where $F_2^N(x, Q_0^2)$ is given in (3.15). Recently E665 Collaboration has measured the nuclear shadowing effect in muon scatterings off ^{40}Ca and ^{208}Pb at low x [2]. In general, the small x data are measured at low Q^2 , e.g., for $x = 6 \times 10^{-4}$ the average $\langle Q^2 \rangle = 0.26$ GeV² while $x = 6 \times 10^{-3}$ corresponds to $\langle Q^2 \rangle = 1.35$ GeV². We parametrize the initial shadowing ratio $R_0^q(x)$ at $Q_0^2 = 0.4$ GeV² and use (5.3) to calculate the nuclear structure function at the measured $\langle Q^2 \rangle$ values at different x values. The nuclear shadowing ratio is defined by

$$\begin{aligned} R_q(x, Q^2) &= \frac{F_2^A(x, Q^2)}{A F_2^N(x, Q^2)} \\ &= \frac{R_0^q(x) F_2^N(x, Q_0^2) + \Delta F_2^A(x; Q^2, Q_0^2)}{F_2^N(x, Q_0^2) + \Delta F_2^N(x; Q^2, Q_0^2)}, \end{aligned} \quad (5.5)$$

where $\Delta F_2 \equiv F_2 - F_2(Q_0^2)$ can be explicitly calculated by performing the double integration over x' and Q'^2 in (5.1). The results for ^{40}Ca and ^{208}Pb are shown in Fig. 4.

The lower panels of Fig. 4 show our parametrizations of initial shadowing ratios at Q_0^2 evolved to the measured $\langle Q^2 \rangle$ compared to the experimental data from E665. For $\langle Q^2 \rangle < Q_0^2$, we take it to be at the minimal scale Q_0^2 . As is evident from the comparison, our parameterizations faithfully represent the experimental data at small

x . The shadowing ratios $R_q(x, Q^2)$ at high values of Q^2 are shown in the upper panels of Fig. 4.

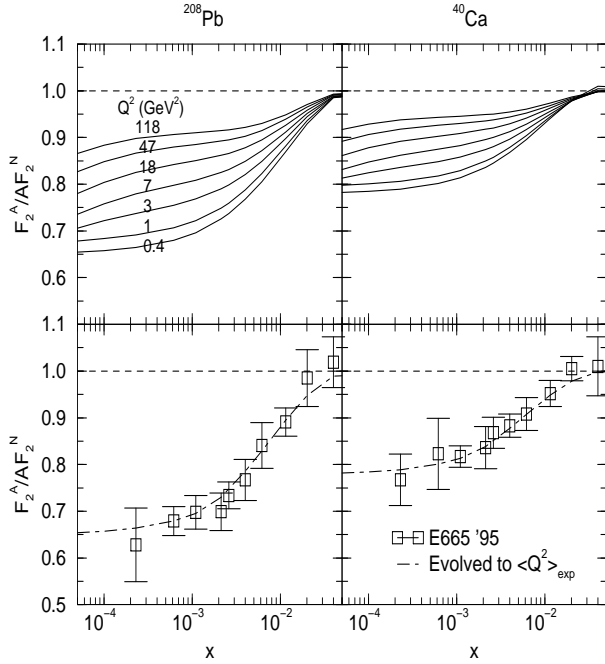


FIG. 4. The x -dependence of nuclear quark shadowing ratio $R_q = F_2^A / (AF_2^N)$ at various Q^2 for ^{208}Pb and ^{40}Ca . The lower panels represent the parameterizations of initial shadowing ratios evolved to the experimental $\langle Q^2 \rangle_{\text{exp}}$ values. The non-saturation of $R_q(x)$ as x decreases at large Q^2 is the feature of the perturbative shadowing mechanism.

We note that at large Q^2 the nuclear shadowing effect is reduced but does not diminish, i.e. it is not a higher twist effect. This can be understood as the interplay between the perturbative and the non-perturbative shadowing mechanisms. The nuclear quark density is initially shadowed by R_q^0 at Q_0^2 compared to the free nucleon case due to some non-perturbative mechanism such as coherent scatterings of the ρ -meson as discussed in the VMD model [15]. As Q^2 increases from Q_0^2 , the nucleon structure function increases by $\Delta F_2^N(x; Q^2, Q_0^2)$ as governed by the GLAP evolution equation in the DLA. If the nuclear F_2^A increases by the same amount (times A), i.e., we neglect the multiple scattering effect and evolve it according to the same GLAP equation, the initial shadowing effect in (5.5) decreases quickly due to the strong scaling violation at low Q^2 ($\Delta F_2^N(x; Q^2, Q_0^2)$ is not small compared to $F_2^N(x, Q_0^2)$). This is illustrated in Fig. 5 where the shadowing ratio is calculated by taking the first term in the expansion $[\dots]$ in (5.1) and is plotted as a function of Q^2 at $x = 10^{-4}$. The shadowing effect disappears quickly when both nucleon and nuclear structure functions evolve according to the GLAP equation.

However, because xg_N^{DLA} increases rapidly as Q^2 increases, the growth of the gluon density in a nucleon compensates for the suppression due to the smallness of

the size of the $q\bar{q}$ pair. As a result, κ_q is not small in the semihard Q^2 region. In fact, κ_q increases as Q^2 increases from Q_0^2 to 2 GeV² and becomes greater than 1. The perturbative rescattering effect becomes important and needs to be taken into account in the Glauber formalism. The effect of multiple scatterings slows down the Q^2 evolution of F_2^A as compared to F_2^N , i.e.,

$$\Delta F_2^A(x; Q^2, Q_0^2) < \Delta F_2^N(x; Q^2, Q_0^2), \quad (5.6)$$

which provides a perturbative shadowing mechanism beyond Q_0^2 . This is illustrated in Fig. 5 where the Q^2 evolution is indeed slower than the GLAP evolution case. As Q^2 becomes even larger ($Q^2 > 5$ GeV²), κ_q decreases fast and the probability for rescattering becomes small. In this case, both F_2^A and F_2^N evolve slowly and so does the shadowing ratio. Also plotted in Fig. 5 is the double scattering case where we take the first two terms in the expansion

$$[\gamma + \ln \kappa_q + E_1(\kappa_q)] \simeq \kappa_q - \frac{1}{4} \kappa_q^2. \quad (5.7)$$

As it is evident from Fig. 5, the double scattering overestimates the amount of shadowing. Nevertheless, it accounts for most of the multiple scattering effect.

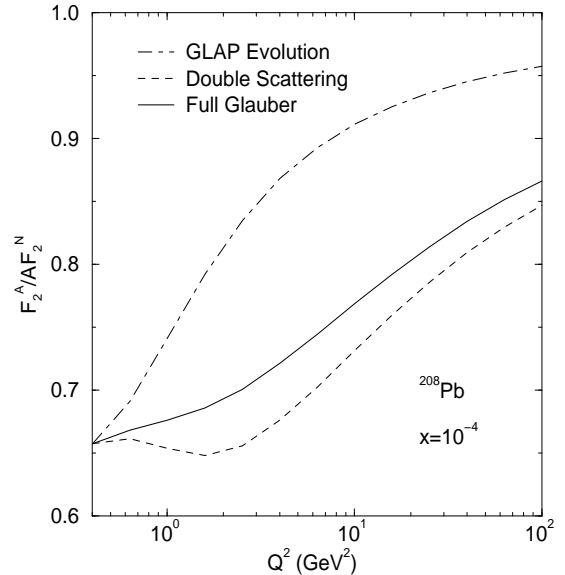


FIG. 5. The Q^2 -dependence of nuclear quark shadowing ratio $R_q = F_2^A / (AF_2^N)$ at $x = 10^{-4}$ for ^{208}Pb .

The interplay between soft physics and the partonic picture of the nuclear shadowing is also evident in the x -dependence of R_q in Fig. 4. The apparent flatness of the shadowing ratio at low Q^2 in the small- x region is altered by the perturbative evolution. This is due to the singular behavior of xg_N^{DLA} as $x \rightarrow 0$ at large Q^2 leading to the strong x -dependence of the effective number of scatterings, $\kappa_q(x)$. Thus, the saturation of the R_q as x decreases is a feature only at low Q^2 (< 2 GeV²) where

the gluon density is not so singular, and we do not expect saturation to happen for higher values of Q^2 .

VI. PREDICTING GLUON SHADOWING

In the previous section, we have emphasized the importance of the interplay between the non-perturbative and perturbative shadowing mechanisms in order to predict the nuclear quark shadowing at large Q^2 . This would suggest that the prediction for the nuclear gluon shadowing is uncertain because there is very little experimental information on the gluon shadowing at low Q^2 . However, as we shall demonstrate below, this is not the case and the gluon shadowing can be unambiguously predicted for large Q^2 in the context of perturbative QCD.

The nuclear gluon distribution can be calculated in the Glauber model similarly to the quark case [13]

$$xg_A(x, Q^2) = xg_A(x, Q_0^2) + \frac{2R_A^2}{\pi^2} \int_x^1 \frac{dx'}{x'} \int_{Q_0^2}^{Q^2} dQ'^2 \times \frac{1}{\tau} [\gamma + \ln(\kappa_g \tau) + E_1(\kappa_g \tau)] , \quad (6.1)$$

The main difference between the quark and gluon cases is different wave functions of the virtual probe and the effective number of scatterings, $\kappa_g = 9\kappa_q/4$ due to different color representations that the quark and the gluon belong to. As a result, the gluon density increases as Q^2 increases 12 times faster than the sea-quark density at small x . The two important effects which make gluon shadowing quite different from quark shadowing are a stronger scaling violation in the semihard scale region and a larger perturbative shadowing effect. This can be seen by considering the shadowing ratio

$$R_g(x, Q^2) = \frac{xg_A(x, Q^2)}{Axg_N(x, Q^2)} \quad (6.2) \\ = \frac{xg_N(x, Q_0^2)R_g^0(x) + \Delta xg_A(x; Q^2, Q_0^2)}{xg_N(x, Q_0^2) + \Delta xg_N(x; Q^2, Q_0^2)} ,$$

where $R_g^0(x)$ is the initial shadowing ratio at Q_0^2 and $\Delta xg(x; Q^2, Q_0^2)$ is the change of the gluon distribution as the scale changes from Q_0^2 to Q^2 . The strong scaling violation due to a larger κ_g at small x causes $\Delta xg_N(x; Q^2, Q_0^2) \gg xg_N(x, Q_0^2)$ as Q^2 becomes greater than $1 \sim 2 \text{ GeV}^2$. The dependence of $R_g(x, Q^2)$ on the initial condition $R_g^0(x)$ diminishes and the perturbative shadowing mechanism takes over, i.e.

$$R_g(x, Q^2) \rightarrow \frac{\Delta xg_A(x; Q^2, Q_0^2)}{\Delta xg_N(x; Q^2, Q_0^2)} , \quad (6.3)$$

for $Q^2 > 2 \text{ GeV}^2$.

The above statement can be made more rigorous by taking a partial derivative of (6.2) with respect to $\ln Q^2$ at fixed x

$$\frac{\partial R_g(x, Q^2)}{\partial \ln Q^2} = \gamma(x, Q^2) [R_g^{\text{PT}}(x, Q^2) - R_g(x, Q^2)] , \quad (6.4)$$

where the anomalous dimension $\gamma(x, Q^2)$ and the so-called perturbative shadowing ratio R_g^{PT} are defined

$$\gamma(x, Q^2) = \frac{\partial \ln xg_N(x, Q^2)}{\partial \ln Q^2} \\ R_g^{\text{PT}}(x, Q^2) = \frac{\partial xg_A(x, Q^2)/\partial \ln Q^2}{A \partial xg_N(x, Q^2)/\partial \ln Q^2} . \quad (6.5)$$

Note that R_g^{PT} is the ratio of the derivative of xg_A to that of xg_N , which is independent of the initial shadowing ratio and can be calculated perturbatively. In the small- x region

$$R_g^{\text{PT}} \simeq \frac{\gamma + \ln \kappa_g + E_1(\kappa_g)}{\kappa_g} = 1 - \frac{\kappa_g}{4} + \frac{\kappa_g^2}{18} - \dots . \quad (6.6)$$

The interesting feature of (6.4) is the negative sign in front of R_g on the right hand side such that it is self-stabilizing. If $R_g < R_g^{\text{PT}}$ at Q^2 and $\partial R_g/\partial \ln Q^2 > 0$, the shadowing ratio increases with Q^2 ; while for $R_g > R_g^{\text{PT}}$, the shadowing ratio decreases with Q^2 . As a result, the Q^2 -evolution of R_g is such that it is always in the process of approaching R_g^{PT} . Because R_g^{PT} also changes with Q^2 , the Q^2 -evolution of R_g never stops. The anomalous dimension $\gamma(x, Q^2)$ determines how fast R_g is approaching R_g^{PT} .

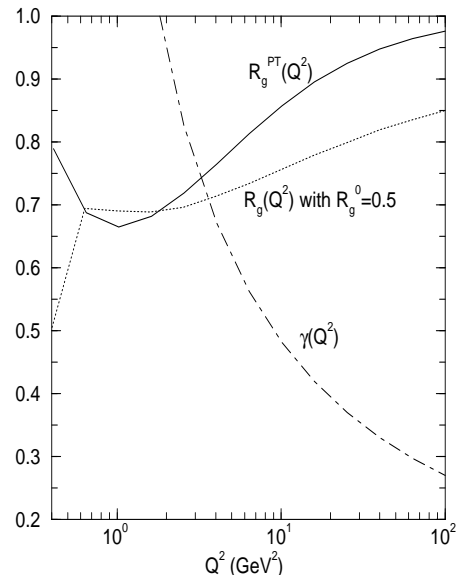


FIG. 6. The Q^2 -dependence of the anomalous dimension $\gamma(x, Q^2)$ and the perturbative shadowing ratio $R_g^{\text{PT}}(x, Q^2)$ at $x = 10^{-4}$ for ^{208}Pb . Also plotted is the shadowing ratio R_g with an initial condition $R_g^0 = 0.5$.

Introduce an important scale $Q_{\text{SH}}^2 = 3 \text{ GeV}^2$ (“SH” stands for “semihard”) where $\gamma(x, Q_{\text{SH}}^2) \simeq O(1)$ for small

values of x ($10^{-5} < x < 10^{-3}$). In the semihard region $Q_0^2 < Q^2 < Q_{\text{SH}}^2$, $\gamma(x, Q^2)$ is large and R_g approaches $R_g^{\text{PT}}(x, Q_{\text{SH}}^2)$ fast regardless of what the initial shadowing is at Q_0^2 . It is precisely in this region that κ_g is large and (6.6) gives a large shadowing correction. As $Q^2 > Q_{\text{SH}}^2$, the anomalous dimension γ gets small and in the meantime R_g^{PT} approaches 1 rather quickly, the shadowing ratio R_g evolves slowly. Thus, the behavior of the Q^2 -evolution of the gluon shadowing can be understood by the interplay between the anomalous dimension of the nucleon gluon structure function and the perturbative shadowing mechanism.

In Fig. 6 we show the Q^2 -behavior of $\gamma(x, Q^2)$ and $R_g^{\text{PT}}(x, Q^2)$ at $x = 10^{-4}$ for ^{208}Pb . The evolution of the shadowing ratio R_g with an initial condition $R_g^0(x) = 0.5$ is also plotted to illustrate the evolution governed by (6.4).

To study the sensitivity of the shadowing ratio on the initial condition, one can solve (6.4) explicitly by making a transformation $R_g = R'_g \exp[-\int \gamma(x, t') dt']$ where $t = \ln Q^2$. Then R'_g can be directly integrated out which yields

$$R_g(x, t) = R_g(x, t_0) e^{-\int_{t_0}^t \gamma(x, t') dt'} + e^{-\int_{t_0}^t \gamma(x, t') dt'} \times \int_{t_0}^t \gamma(x, t') e^{\int_{t_0}^{t'} \gamma(x, t'') dt''} R_g^{\text{PT}}(x, t') dt'. \quad (6.7)$$

In the absence of perturbative shadowing, i.e. $R_g^{\text{PT}} = 1$, the integral in (6.7) can be done exactly leading to a pure GLAP evolution

$$R_g^{\text{GLAP}}(x, t) = 1 - [1 - R_g(x, t_0)] e^{-\int_{t_0}^t \gamma(x, t') dt'}. \quad (6.8)$$

In the DLA, the integration of $\gamma(x, t)$ yields

$$e^{-\int_{t_0}^t \gamma(x, t') dt'} = \frac{x g_N^{\text{DLA}}(x, t_0)}{x g_N^{\text{DLA}}(x, t)} = \frac{1}{I_0(y)} \quad (6.9)$$

where y is defined in (3.13). The factor $1/I_0(y)$ suppresses the initial shadowing $R_g(x, t_0)$ quickly for large $t > t_{\text{SH}} = \ln Q_{\text{SH}}^2$. The integration in (6.9) picks up most important contributions in the region $t_0 < t < t_{\text{SH}}$. Therefore, $R_g^{\text{GLAP}} \rightarrow 1$ quickly as $t > t_{\text{SH}}$. In the presence of perturbative shadowing, i.e. $R_g^{\text{PT}} < 1$, $R_g(x, t)$ at large t is mainly determined by the second term in (6.7) and it depends only on γ and R_g^{PT} , especially in the small- x region.

Fig. 7 demonstrates the stabilization of the gluon shadowing for any initial conditions as Q^2 increases at various values of x for ^{208}Pb . The shaded regions indicate the maximal uncertainty in predicting the gluon shadowing as they are bounded by two extreme initial conditions: $R_g^0(x) = 1$ and $R_g^0(x) = 0$ for all values of x . One can almost uniquely determine the amount of the gluon shadowing for $Q^2 > 3 \text{ GeV}^2$. In general, the uncertainty gets

bigger as x gets larger due to a weaker scaling violation, which is evident in Fig. 7.

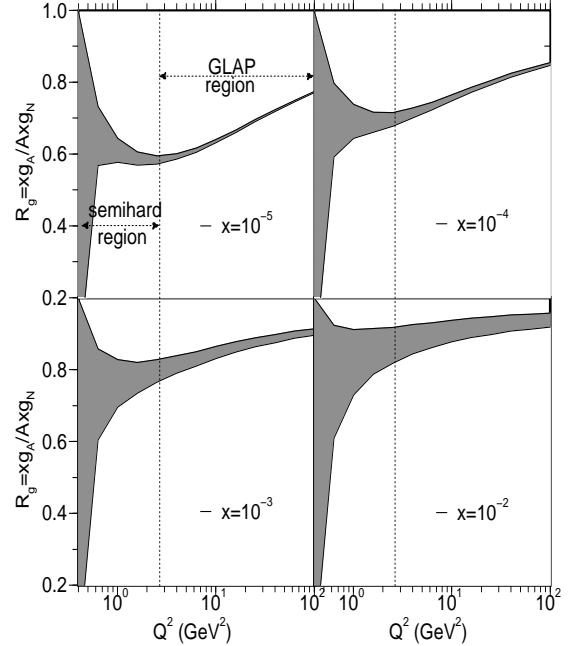


FIG. 7. The maximal uncertainty in predicting the gluon shadowing due to initial conditions. The shaded regions are bounded by two extreme initial conditions: $R_g^0(x) = 1$ and $R_g^0(x) = 0$.

Neglecting the first term in (6.7) and approximating the perturbative shadowing by $R_g^{\text{PT}} = R_g^{\text{PT}}(Q_{\text{SH}}^2)$ for $Q_0^2 < Q^2 < Q_{\text{SH}}^2$ and $R_g^{\text{PT}} = 1$ for $Q^2 > Q_{\text{SH}}^2$, one obtains from (6.7) the shadowing ratio for $Q^2 > Q_{\text{SH}}^2$

$$R_g(x, t) = 1 - [1 - R_g^{\text{PT}}(x, t_{\text{SH}})] e^{-\int_{t_{\text{SH}}}^t \gamma(x, t') dt'}. \quad (6.10)$$

Comparing (6.10) with (6.7), one notices that solution (6.10) is just solution (6.7) with a new initial condition $R_g^0 = R_g^{\text{PT}}(x, Q_{\text{SH}}^2)$ and Q_0^2 replaced by Q_{SH}^2 . The difference is that the evolution factor $\exp[-\int]$ no longer falls rapidly and R_g evolves rather slowly. Thus, the Q^2 -behavior of gluon shadowing at large Q^2 can be roughly described by an initial condition at Q_{SH}^2 followed by a GLAP evolution. The important point is that the initial condition at $Q^2 = Q_{\text{SH}}^2$ is pre-determined by the perturbative shadowing. Our main conclusion is that even though $R_g^{\text{PT}}(x, Q^2)$ approaches 1 quickly as Q^2 increases beyond Q_{SH}^2 (a higher twist effect), the shadowing ratio at large Q^2 is still governed by the perturbative shadowing at the *semihard scale*, namely $R_g^{\text{PT}}(x, Q_{\text{SH}}^2)$.

The x -dependence of the gluon shadowing can also be predicted as long as $Q^2 > Q_{\text{SH}}^2$ where the influence of the initial condition is minimal. Fig. 8 shows the x -dependence of the gluon shadowing ratio at various Q^2 values. The shaded region is bounded by the distributions calculated using two drastically different initial conditions $R_g^0(x) = 0$ and $R_g^0(x) = 1$. It is clear that the

shape of the distribution is quite robust in the small- x region regardless of what initial conditions one may choose. Due to the perturbative nature of the shadowing, these distributions do not exhibit a saturation as x decreases. This is related to the singular behavior of the nucleon gluon distribution at large Q^2 and small x . As long as the nucleon gluon density does not saturates at small x , the shadowing ratio does not saturate either. This is in accordance with the observation by Eskola, Qiu and Wang in the context of the gluon recombination model [8]. The rapid Q^2 -evolution of the gluon shadowing ratio in the low Q^2 region found by Eskola [16] can be understood in our approach as the quick onset of the perturbative shadowing. In Eskola's approach some shadowing persists even at $Q^2 = 100 \text{ GeV}^2$ which can also be understood in our picture as the region of fully developed GLAP evolution. We note that multiple scatterings inside the nucleon are also possible in the region of very small x , where the eikonalization of the nucleon cross section is needed. However, in this region, the DLA breaks down and a BFKL resummation is necessary.

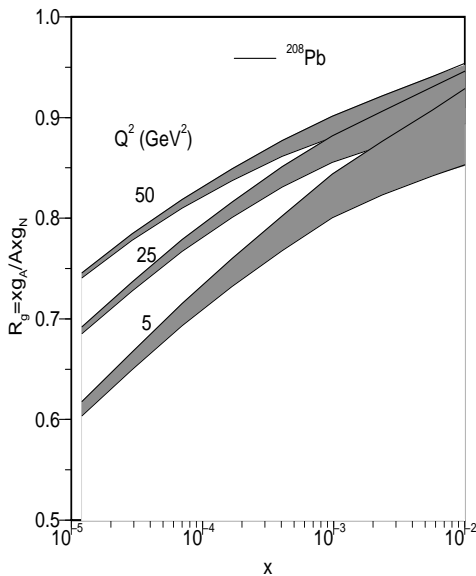


FIG. 8. The x -dependence of the gluon shadowing ratio at various Q^2 values. The shaded region indicates the uncertainty due to the initial conditions.

VII. GLUON SHADOWING AT FIXED IMPACT PARAMETER

So far we have confined ourselves to the impact parameter averaged nuclear structure function. However, in the binary approximation of hard scattering processes in pA and AA collisions, one has to calculate the parton cross section at the nucleon-nucleon level at each impact parameter. In addition, to enhance the possible signal of a quark-gluon plasma in heavy-ion collisions, one triggers

on central events where the impact parameter is small (e.g. $b < 2 \text{ fm}$). It is thus necessary to study the impact parameter dependence of the nuclear shadowing effect.

Intuitively, one expects the nuclear shadowing effect to depend on the local nuclear thickness at a given impact parameter. In the Glauber approach, the effective number of scatterings is the product of the cross section and the nuclear thickness function. Since the shadowing is a non-linear effect in the effective number of scatterings, the impact parameter dependent shadowing ratio cannot be factorized into a product of an average shadowing ratio and the nuclear thickness function [27].

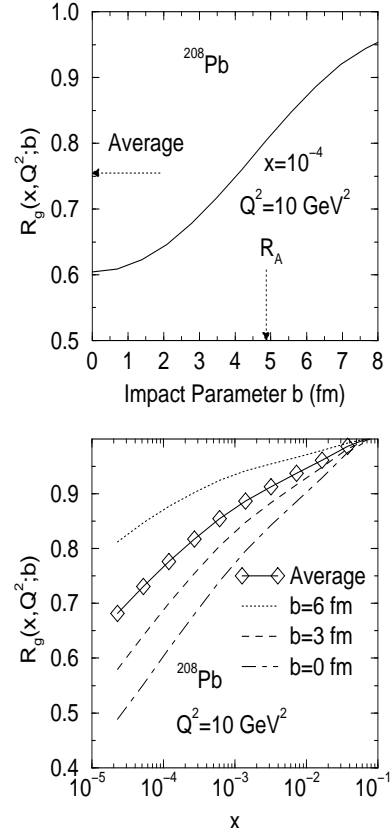


FIG. 9. The impact parameter dependent gluon shadowing ratio calculated assuming $R_g^0(x, Q_0^2; b) = 1$ for any b . The upper panel is the shadowing ratio as function of b at $x = 10^{-4}$ and $Q^2 = 10 \text{ GeV}^2$. The lower panel shows the x -dependence of the shadowing ratio at $Q^2 = 10 \text{ GeV}^2$ and various values of b .

The impact parameter dependent nuclear structure function $x\tilde{g}_A(x, Q^2; \mathbf{b})$ is defined as

$$xg_A(x, Q^2) = \int d^2\mathbf{b} x\tilde{g}_A(x, Q^2; \mathbf{b}). \quad (7.1)$$

Comparing (7.1) with (4.7), one finds

$$x\tilde{g}_A(x, Q^2; \mathbf{b}) = x\tilde{g}_A(x, Q_0^2; \mathbf{b}) + \frac{4}{\pi^3} \int_x^1 \frac{dx'}{x'} \int_{Q_0^2}^{Q^2} dQ'^2 \times 2 \left[1 - e^{-\sigma_{ggN} T_A(\mathbf{b})/2} \right], \quad (7.2)$$

where $x\tilde{g}_A(x, Q_0^2; \mathbf{b})$ is the initial condition at fixed impact parameter \mathbf{b} . As shown in the previous section, the prediction for gluon shadowing ratio at $Q^2 \geq 3\text{GeV}^2$ does not depend on the initial condition. We take the initial shadowing ratio to be 1 for all \mathbf{b} 's, i.e. no initial shadowing. The impact parameter dependent shadowing ratio is thus defined

$$R_g(x, Q^2; \mathbf{b}) = \frac{x\tilde{g}_A(x, Q^2; \mathbf{b})}{T_A(\mathbf{b})xg_N(x, Q^2)}. \quad (7.3)$$

In Fig. 9 we show the gluon shadowing at various impact parameters. The upper panel is the shadowing ratio as function of b at $x = 10^{-4}$ and $Q^2 = 10\text{GeV}^2$. The parton density is more suppressed at a small impact parameter. The x -dependence of the impact parameter dependent shadowing ratio is also shown in the lower panel of Fig. 9.

VIII. CONCLUSIONS

We have studied the nuclear shadowing mechanism in the context of perturbative QCD and the Glauber multiple scattering model. The nuclear shadowing phenomenon is a consequence of the coherent parton multiple scatterings. While the quark density shadowing arises from an interplay between the ‘‘soft’’ and the semihard QCD processes, the gluon shadowing is largely driven by a perturbative shadowing mechanism due to the strong scaling violation in the small- x region. The gluon shadowing is thus a robust phenomenon at large Q^2 and can be unambiguously predicted by perturbative QCD.

The scale dependence of the nucleon structure function has been used to put a stringent constraint on the gluon density inside the nucleon in the double logarithm approximation. It is shown that the strong scaling violation of the nucleon structure function in the semihard momentum transfer region $0.8 \leq Q^2 \leq 3\text{GeV}^2$ at small x can be reliably described by perturbative QCD and is a central key to the understanding of the scale dependence of the nuclear shadowing effect.

We have also studied the impact parameter dependence of gluon shadowing and shown that it is a non-linear effect in the nuclear thickness function. It is important to correctly incorporate the impact parameter dependence of the nuclear structure function when one calculates the QCD processes such as minijet production and J/ψ production in the central nucleus collisions.

ACKNOWLEDGMENTS

This work was supported through the U.S. Department of Energy under Contracts Nos. DE-FG03-93ER40792 and DE-FG03-85ER40213.

APPENDIX: PARAMETRIZATION OF GLUON SHADOWING AND ITS IMPACT PARAMETER DEPENDENCE

Motivated by our studies of the gluon shadowing at $Q^2 > Q_{\text{SH}}^2$, we parametrize the gluon shadowing ratio in the following way:

$$R_g(x, Q^2) = 1 - [1 - R_g^{\text{PT}}(x, Q_{\text{SH}}^2)] \times [1 - a_0 \ln Q^2 / Q_{\text{SH}}^2], \quad (1)$$

where $Q_{\text{SH}}^2 = 3\text{GeV}^2$, $a_0 = 0.3$ and

$$R_g^{\text{PT}}(x, Q_{\text{SH}}^2) = 1 - a_1 A^\alpha x^{-\lambda} (1-x)^\beta, \quad (2)$$

where A is the atomic number of the nucleus and

$$a_1 = 0.0249; \quad \alpha = 0.18; \quad \lambda = 0.162; \quad \beta = 18. \quad (3)$$

The impact parameter dependent ratio $R_g(x, Q^2; \mathbf{b})$ is parametrized via a b -averaged ratio $R_g(x, Q^2)$

$$R_g(x, Q^2; \mathbf{b}) = 1 - c_0(1 + c_1 A^{-\alpha'} b^2) \times \exp[-A^{-\alpha'} b^2 / c_2] (1 - R_g(x, Q^2)), \quad (4)$$

where b is the impact parameter in fm and

$$c_0 = 1.7; \quad c_1 = 0.043; \quad \alpha' = 0.11; \quad c_2 = 11.45. \quad (5)$$

Note that these parametrizations are valid for $Q^2 > Q_{\text{SH}}^2$ and $x < 10^{-2}$.

-
- [1] NMC Collaboration, P. Amaudruz *et al.*, Z. Phys. C **51**, 387 (1991); Z. Phys. C **53**, 73 (1992); Phys. Lett. B **295**, 195 (1992); NMC Collaboration, M. Arneodo *et al.*, Nucl. Phys. B **441**, 12 (1995).
 - [2] E665 Collaboration, M.R. Adams *et al.*, Phys. Rev. Lett. **68**, 3266 (1992); Phys. Lett. B **287**, 375 (1992); Z. Phys. C **67**, 403 (1995).
 - [3] D. Alde *et al.*, Phys. Rev. Lett. **66**, 133 (1991).
 - [4] S. Gavin and J. Milana, Phys. Rev. Lett. **68**, 1834; C.J. Benesh, J. Qiu and J.P. Vary, Phys. Rev. C **50**, 1015 (1994).
 - [5] B. Badelek and J. Kwieciński, Rev. Mod. Phys. **64**, 927 (1992); M. Arneodo, Phys. Rep. **240**, 301 (1994).
 - [6] L.V. Gribov, E.M. Levin and M.G. Ryskin, Phys. Rep. **100**, 1 (1983); E. Laenen and E. Levin, Nucl. Phys. B **451**, 207 (1995).
 - [7] A.H. Mueller and J. Qiu, Nucl. Phys. B **268**, 427 (1986); J. Qiu, Nucl. Phys. B **291**, 746 (1987).
 - [8] K.J. Eskola, J. Qiu and X.-N. Wang, Phys. Rev. Lett. **72**, 36 (1994).
 - [9] L. Frankfurt and M. Strikman, Nucl. Phys. B **316**, 340 (1989); L. Frankfurt, M. Strikman and S. Liuti, Phys. Rev. Lett. **65**, 1725 (1990).

- [10] S.J. Brodsky and H.J. Lu, Phys. Rev. Lett. **64**, 1342 (1990).
- [11] N.N. Nikolaev, Z. Phys. C **32**, 537 (1986); N.N. Nikolaev and B.G. Zakharov, Phys. Lett. B **260**, 414 (1991); Z. Phys. C **49**, 607 (1991).
- [12] A.H. Mueller, Nucl. Phys. B **335**, 115 (1990).
- [13] A.L. Ayala F, M.B. Gay Ducati and E.M. Levin, e-Print Archive: hep-ph/9604383.
- [14] V.N. Gribov and L.N. Lipatov, Sov. J. Nucl. Phys. **15**, 438 (1972); G. Altarelli and G. Parisi, Nucl. Phys. B **126**, 298 (1977); Yu.L. Dokshitzer, Sov. Phys. JETP **46**, 641 (1977).
- [15] see e.g., G. Piller, W. Ratzka and W. Weise, Z. Phys. A **352**, 427 (1995); T.H. Bauer, R.D. Spital and D.R. Yennie and F.M. Pipkin, Rev. Mod. Phys. **50**, 261 (1978).
- [16] K.J. Eskola, Nucl. Phys. B **400**, 240 (1993).
- [17] A.D. Martin, R.G. Roberts and W.J. Stirling, Phys. Lett. B **387**, 419 (1996); H.L. Lai, J. Huston, S. Kuhlmann, F. Olness, J. Owens, D. Soper, W.K. Tung and H. Weerts, Phys. Rev. D **55**, 1280 (1997); M. Glueck, E. Reya and A. Vogt, Z. Phys. C **67**, 433 (1995).
- [18] R.J. Glauber, in *Lectures in theoretical physics*, ed. W.E. Brittin *et al.* (Interscience Publishers, New York, 1959); R.J. Glauber and G. Matthiae, Nucl. Phys. B **21**, 135 (1970).
- [19] E.A. Kuraev, L.N. Lipatov and V.S. Fadin, Sov. Phys. JETP **45**, 199 (1977); Ya.Ya. Balitskii and L.V. Lipatov, Sov. J. Nucl. Phys. **28**, 822 (1978); L.N. Lipatov, Sov. Phys. JETP **63**, 904 (1986).
- [20] L. McLerran and R. Venugopalan, Phys. Rev. D **49**, 2233 (1994); A. Kovner, L. McLerran and H. Weigert, Phys. Rev. D **52**, 6231 (1995); D **52**, 3809 (1995).
- [21] A.J. Brodsky and A.H. Mueller, Phys. Lett. B **206**, 685 (1988); G. Farrar, L. Frankfurt, M. Strikman and H. Liu, Phys. Rev. Lett. **64**, 1996 (1990).
- [22] For recent studies, see R.K. Ellis, Z. Kunszt and E.M. Levin, Nucl. Phys. B **420**, 517 (1994); R.D. Ball and S. Forte, Phys. Lett. B **335**, 77 (1994).
- [23] B. Blattel, G. Baym, L. Frankfurt and M. Strikman, Phys. Rev. Lett. **71**, 896 (1993); L. Frankfurt, G. Miller and M. Strikman, Phys. Lett. B **304**, 1 (1993).
- [24] H1 Collaboration, T. Ahmed *et al.*, Nucl. Phys. B **470**, 3 (1996); H1 Collaboration, C. Adloff *et al.*, DESY-97-042, e-Print Archive: hep-ex/9703012.
- [25] A. Donnachie and P.V. Landshoff, Phys. Lett. B **191**, 309 (1987); Z. Phys. C **61**, 139 (1994).
- [26] B. Kopeliovich and B. Povh, Phys. Lett. B **367**, 329 (1996).
- [27] K.J. Eskola, Z. Phys. C **51**, 633 (1991).